

## RCCM2–BATS Model over Tropical South America: Applications to Tropical Deforestation

ANDREA N. HAHMANN AND ROBERT E. DICKINSON

*Institute of Atmospheric Physics, The University of Arizona, Tucson, Arizona*

(Manuscript received 10 June 1996, in final form 2 December 1996)

### ABSTRACT

A multiyear simulation of the global climate uses a revised version of the National Center for Atmospheric Research (NCAR) Community Climate Model Version 2 (CCM2) coupled to the Biosphere–Atmosphere Transfer Scheme (BATS). It is compared with global and rain gauge precipitation climatologies to evaluate precipitation fields and European Centre for Medium-Range Forecasts analyses to evaluate the atmospheric circulation. The near-surface climate is compared with data from Amazonian field campaigns. The model simulation of the South American climate agrees closely with the observational record and is much improved from past simulations with previous versions of the NCAR Community Climate Model over this portion of the Tropics.

The model is then used to study the local and regional response to tropical deforestation over Amazonia. In addition to the standard deforestation forcing, consisting mainly of increased albedo and decreased roughness length, two additional sensitivity experiments were conducted to assess the individual contributions from these forcings to the deforestation changes. The standard deforestation simulation shows slight increases in annually averaged surface temperature ( $+1^{\circ}\text{C}$ ) and reductions in annually averaged precipitation and evaporation ( $-363$  and  $-149$  mm  $\text{yr}^{-1}$ , respectively).

As expected, increases in surface albedo over Amazonia produce a reduction in net downward solar radiation at the surface and consequently a reduction in net surface radiation and surface latent heat flux. The roughness decrease, on the other hand, reduces the surface latent heat fluxes through decreases in the surface drag coefficient. The regional changes in moisture convergence and precipitation during the Amazonian wet season display a shift in the area of maximum precipitation rather than an overall decrease over the deforested area. These shifts are evidently produced by a combination of the changes in the low-level circulation and a decrease in the efficiency of precipitation recycling within Amazonia.

### 1. Introduction

With the world's largest rain forest, the Amazon is of great ecological and climatic importance. Its climate is a major element of the overall tropical rainfall system. Exploring how Amazon deforestation affects climate improves our understanding of the interactions between land-surface processes and the climate system. It also helps us to better define the processes and details needed by the land component of climate models.

Dramatic changes in vegetation cover, such as that from tropical deforestation, are expected to affect the climate at some scale, but how in detail tropical forests affect precipitation and other climate elements is unclear. The spatial extent of present deforestation is still too small to induce large-scale changes (Chu et al. 1994), being confined to small areas at local sites (e.g., Bastable et al. 1993; Culf et al. 1995; Wright et al. 1996).

Hence, atmospheric scientists use a hierarchy of numerical models to study the sensitivity of climate to tropical deforestation, and in particular, a large number of general circulation models (GCMs) have been used to analyze the effects of tropical deforestation on regional climate (reviewed in Henderson-Sellers et al. 1993; McGuffie et al. 1995). Most such studies find that extreme tropical deforestation (i.e., the complete transformation of all the area covered by tropical forest into grassland) in Amazonia would result in a warmer and drier climate in this region. Substantial differences exist between the different models in the atmospheric parameterizations and among their simulations as to the magnitude, sign, and other details of the changes (Table 1), especially with regard to the moisture convergence (i.e., precipitation minus evaporation).

Three factors largely control the impact of deforestation: albedo, evaporation, and surface roughness length (Sellers 1992). Most of the recent GCM deforestation studies presented in Table 1 modified the surface boundary conditions to account for the change in all three of these parameters. Some, however, have also estimated their individual effects. In particular, Lean and Warrilow (1989) investigated the changes due to albedo

---

*Corresponding author address:* Dr. Andrea N. Hahmann, Institute of Atmospheric Physics, PAS Building 81, The University of Arizona, Tucson, AZ 85721.  
E-mail: hahmann@vortex.atmo.arizona.edu

TABLE 1. Annual regional response to tropical deforestation from various GCM studies.

Study	Albedo change	Roughness change	$\Delta T$ ( $^{\circ}C$ )	$\Delta P$ (mm)	$\Delta E$ (mm)	Change in moisture convergence
Dickinson and Henderson-Sellers (1988)	0.12/0.19	2.00/0.05	+3.0	0	-200	Inc.
Lean and Warrilow (1989)	0.136/0.188	0.79/0.04	+2.4	-490	-310	Dec
Nobre et al. (1991)	0.13/0.20	2.65/0.08	+2.5	-643	-496	Dec
Dickinson and Kennedy (1992)	0.12/0.19	2.00/0.05	+0.6	-511	-256	Dec
Mylne and Rowntree (1991)	0.135/0.200	—	-0.1	-335	-176	Dec
Henderson-Sellers et al. (1993)	0.12/0.19	2.0/0.2	+0.6	-588	-232	Dec
Lean and Rowntree (1993)	0.136/0.188	0.79/0.04	+2.1	-296	-201	Dec
Pitman et al. (1993)	0.12/0.19	2.00/0.05	+0.7	-603	-207	Dec
Polcher and Laval (1994a)	0.098/0.177	2.30/0.06	+3.8	+394	-985	Inc.
Polcher and Laval (1994b)	0.135/0.216	2.30/0.06	-0.1	-186	-128	Dec
Sud et al. (1996)	0.092/0.142	2.65/0.08	+2.0	-540	-445	Dec
McGuffie et al. (1995)	0.12/0.19	2.0/0.2	+0.3	-437	-231	Dec
Lean et al. (1996)	0.13/0.18	2.10/0.03	+2.3	-157	-296	Inc.
Manzi and Planton (1996)	0.13/0.20	2.00/0.06	-0.5	-146	-113	Dec
This experiment	0.12/0.19	2.00/0.05	+1.0	-363	-149	Dec

and roughness alone using separate 8-month simulations and concluded that the decrease in roughness dominated the reduction in evaporation, whereas the increased albedo was the main cause of a decrease in moisture flux convergence determining the simulated decrease in precipitation. Dirmeyer and Shukla (1994) found in a series of sensitivity experiments, where the rain forest over South America was replaced by grassland and net surface albedos were modified from the control tropical forest value to 0.06 and 0.09 lighter, that if surface albedo was not increased appreciably (by more than 0.03), moisture flux convergence driven by the increase in surface temperature could offset the other effects and increase precipitation. Recent simulations by Lean et al. (1996), however, have indicated that the deforested climate is highly dependent on individual parameter changes and strongly influenced by the nonlinear interaction of these changes.

The interpretation of GCM simulations of tropical deforestation is limited by substantial differences among models and different assumptions made by modeling groups. For continuity, this study assumes deforestation changes similar to those in earlier studies with several versions of the National Center for Atmospheric Research (NCAR) Community Climate Model (CCM; Dickinson and Henderson-Sellers 1988; Dickinson and Kennedy 1992; Henderson-Sellers et al. 1993). All these used the Biosphere-Atmosphere Transfer Scheme. This study should provide more realistic and highly resolved precipitation patterns than did previous deforestation studies, which, except for Lean et al. (1996), used lower-resolution models. Section 2 describes the model used in this study. Since we believe that one of the main ingredients for a realistic representation of the effects of tropical deforestation in GCMs is a proper representation of the present climate by the control simulation, an extensive evaluation of the model control climate over South America is

presented in section 3. Section 4 presents the results from the deforestation experiment, while section 5 explores the relative contributions from albedo increase and/or roughness decrease to the deforestation response. Finally, section 6 summarizes and gives further discussion of the results.

## 2. The model

The model used in this study is a revised version of the NCAR CCM Version 2 (CMM2; Hack et al. 1993) coupled to the Biosphere-Atmosphere Transfer Scheme Version 1e (BATS1e; Dickinson et al. 1993), named RCCM2-BATS. It is a global spectral model developed for a standard T42 spectral truncation (approximately equivalent to a  $2.8^{\circ} \times 2.8^{\circ}$  transform grid), with 18 vertical levels and model top at 2.9 mb, and including the boundary layer parameterization of Holtslag and Boville (1993), a simple mass flux scheme developed by Hack (1994), shortwave radiative heating computed using the  $\delta$ -Eddington parameterization with 18 spectral bands (Briegleb 1992), and longwave parameterization developed by Kiehl and Briegleb (1991). The standard CCM2 includes only a minimal treatment of land-surface processes but optional inclusion of BATS can provide more detailed treatment of land.

The standard CCM2 and CCM2-BATS reasonably simulate most of the features of the present climate, except for serious discrepancies in summer for surface radiative fluxes and temperatures over midlatitude continents (Bonan 1994; Hahmann et al. 1995). The parameterization of cloud optical properties was modified (Hahmann et al. 1995) to address these discrepancies by increasing the optical thickness of summer clouds and more realistically representing the equivalent radius of the water cloud drop size distribution accounting for the differences between land and oceanic regions [similar to that of Kiehl (1994)]. Improvements were (a)

TABLE 2. Summary of model simulations.

Simulation	Description	Duration (averaged years)
Stand. CCM2	Standard CCM2	20 yr (years 1–20)
CCM2/BATS	Standard CCM2 + BATS1e	10 yr (years 1–10)
RCCM2/BATS (FOREST)	Standard CCM2 with revisions to cloud properties + BATS1e	10 yr (years 6–15)
DEFOR	RCCM2–BATS + land use changes over Amazonia	8 yr (years 8–15)
ALBEDO	RCCM2–BATS + albedo increase over Amazonia	5 yr (years 8–12)
ROUGH	RCCM2–BATS + roughness reduction over Amazonia	5 yr (years 8–12)

smaller differences in global annually averaged absorbed solar radiation between CCM2–BATS and Earth Radiation Budget Experiment (ERBE) data (from 6.5 to 3.3  $\text{W m}^{-2}$ ) and improved top-of-the-atmosphere (TOA) radiative balance (net radiative flux of 0.5  $\text{W m}^{-2}$  compared to 7.9 and 4.8  $\text{W m}^{-2}$  in the standard CCM2 and CCM2/BATS simulations), (b) better agreement in Northern Hemisphere summer between model and ERBE TOA fluxes (averaging 20  $\text{W m}^{-2}$  in long-

wave and 40  $\text{W m}^{-2}$  in shortwave TOA fluxes in the standard CCM2 and CCM2–BATS simulations) and surface radiation budget (averaging over 60  $\text{W m}^{-2}$  in the CCM2–BATS simulation), and (c) improved summer surface air temperatures. Surface air temperatures in the RCCM2–BATS simulation are 3.1°C warmer over North America and only 0.6°C warmer over Asia than the climatology (Legates and Willmott 1990a) compared to 6.4 and 5.2°C warmer in the CCM2–BATS simulation.

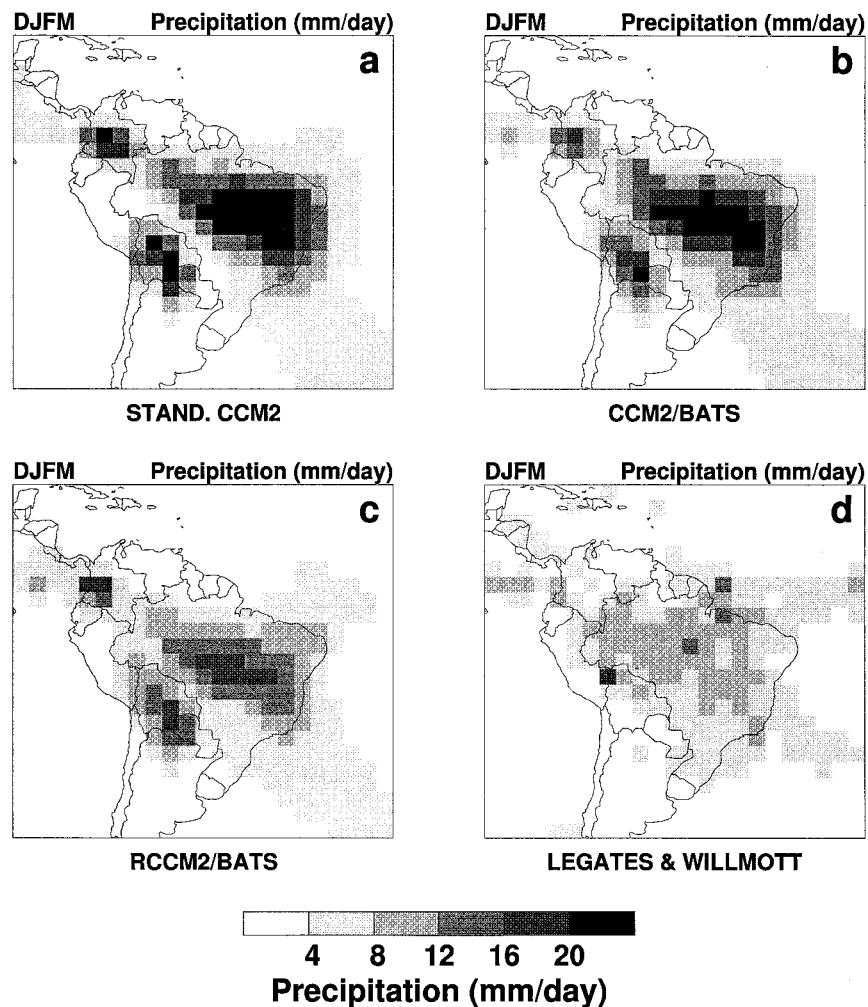


FIG. 1. Ensemble-averaged wet season (December–March) precipitation (mm) simulated by the (a) standard CCM2, (b) CCM2–BATS, (c) RCCM2–BATS models, and (d) the observations by Legates and Willmott (1990b).

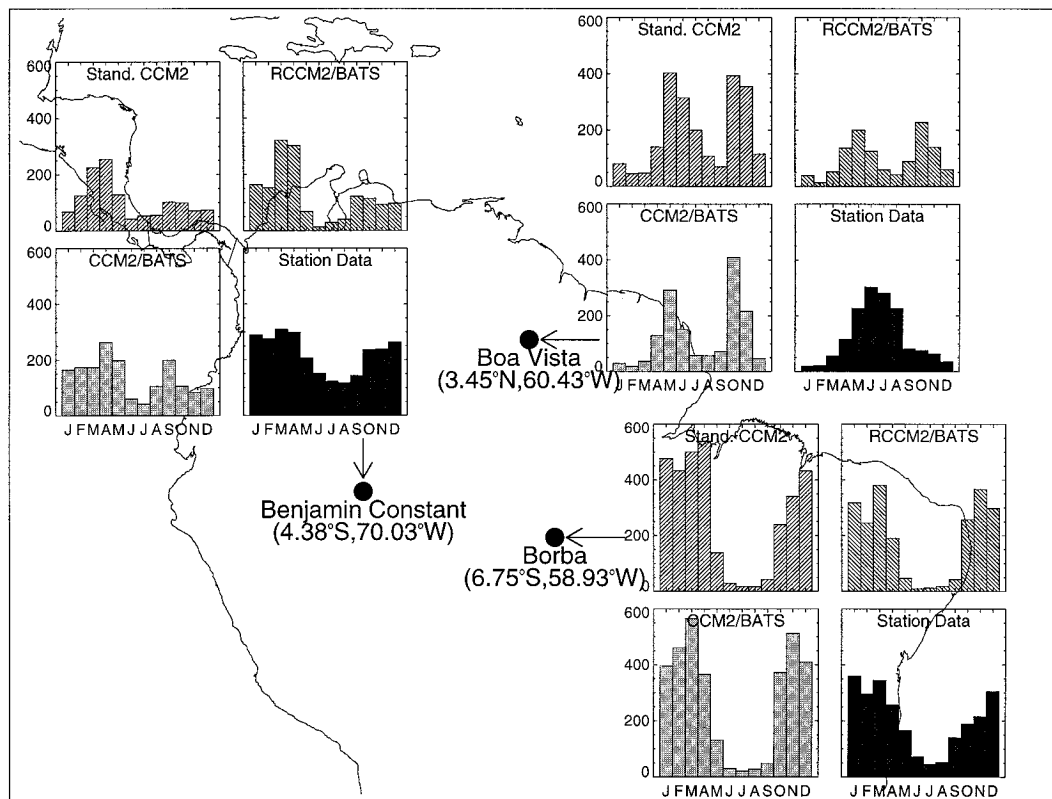


FIG. 2. Comparison of the observed annual cycle of monthly precipitation for selected surface stations in Amazonia with results from various CCM2 simulations.

### 3. The model's climate over South America

Three CCM2 simulations of the global climate (described in Table 2) are analyzed. "Stand. CCM2" is a 20-yr simulation using the standard version of CCM2, and "CCM2-BATS" is a 10-yr simulation of the standard CCM2 coupled to BATS1e. Revisions to the cloud optical properties introduced in the CCM2-BATS model result in the simulation labeled "RCCM2-BATS" in Table 2. All simulations use the same seasonally varying climatological (averages for the period 1950–79) sea surface temperatures (SSTs) of Shea et al. (1992) and ozone profiles.

A large region of intense convection centers over the Amazon Basin in austral summer. Deep convection [seen by the outgoing longwave radiation (OLR) data analyzed by Horel et al. (1989)] resides over the Amazon Basin region from November to March. Associated with this intense convection is a closed anticyclone in the upper troposphere known as the Bolivian high and a downstream trough located over the northeast coast of South America. How a GCM responds to deforestation may depend on how well these features are simulated.

#### a. Precipitation

The precipitation of various versions of CCM2 is validated with three sources of observational data: the glob-

al climatology of Legates and Willmott (1990b), the global terrestrial climatology of Leemans and Cramer (1991), and a 30-yr record of daily precipitation from rain gauge stations for the Brazilian Amazonia (T. Dunne 1995, personal communication).

Figure 1 compares total precipitation in the austral summer (December–March) for the three model simulations with the observational estimates of Legates and Willmott. This 4-month period contains 50%–60% of the annual precipitation in the Amazon Basin. As Hack (1994) indicates, the standard CCM2 model tends to overestimate tropical precipitation (zonally averaged tropical rainfall rates by as much as  $7 \text{ mm day}^{-1}$ ), especially over most of northern South America including the Colombian Andes and eastern Brazil (Fig. 1a). Furthermore, the maximum appears to be shifted eastward toward the semiarid region of northeast Brazil. CCM2-BATS results show moderate improvement, and the RCCM2-BATS simulation displays much closer agreement with observed rainfall rates over this region. Past simulations with CCM1 at R15 resolution have systematically shown an eastward shift in the area of maximum precipitation. Moreover, Shaikh (1996) examined the January precipitation distribution over South America for different horizontal resolutions (varying from R15 to T106) of the standard CCM2. These simulations show a westward shift of the pre-

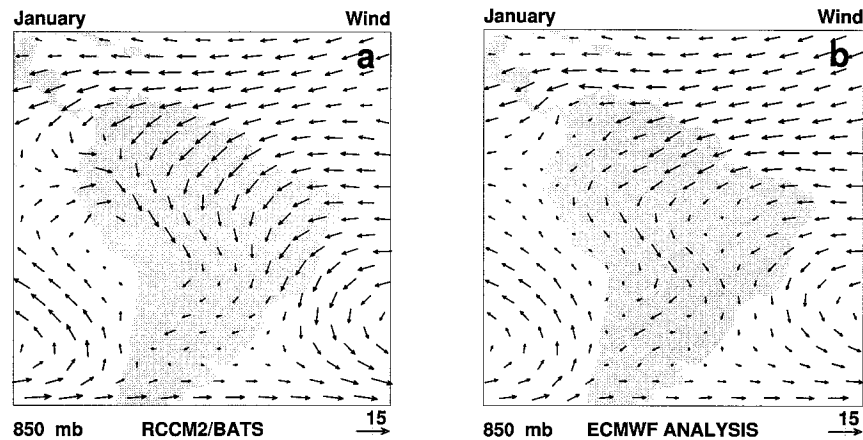


FIG. 3. Comparison of the ensemble-averaged January 850-hPa wind field (a) simulated by the RCM2-BATS model and (b) that from the observationally derived ECMWF analysis. The length of the arrows on the bottom right of each figure represents a wind speed of  $15 \text{ m s}^{-1}$ .

precipitation maximum with resolution increased from R15 to T63, and only the small-scale features improved at T106 resolution. The present T42 resolution appears to be in close agreement with observations, with absolute differences between model and observations of the order of  $5 \text{ mm day}^{-1}$ , primarily a result of the eastward shift of the precipitation maximum rather than of an over- or underestimation of precipitation amounts. Comparison of the model results to an alternate precipitation climatology (Leemans and Cramer 1991) shows that the differences between these two observational estimates (averaging  $2 \text{ mm day}^{-1}$  over the Amazon Basin region) is still substantially smaller than the differences between the model-simulated precipitation (RCCM2-BATS) and the observations. The secondary maximum in precipitation over the Andes Mountains is apparently not seen with such a large horizontal extent in either observational dataset as in all the model simulations. However, observations could

underestimate the amount of rainfall over this mountainous region by largely sampling at lower elevations (Legates and Willmott 1990b).

Three rain gauge stations in Amazonia, Boa Vista ( $3.45^\circ\text{N}$ ,  $60.43^\circ\text{W}$ ), Benjamin Constant ( $4.38^\circ\text{S}$ ,  $70.03^\circ\text{W}$ ), and Borba ( $6.75^\circ\text{S}$ ,  $58.93^\circ\text{W}$ ), have long observational records and are representative of different annual cycles of monthly precipitation. Figure 2 shows their location in the Amazon Basin and compares their annual cycle of precipitation with the three simulations for the model's grid point closest to the respective rain gauge station. The RCM2-BATS simulation captures very well the seasonal cycle of monthly precipitation over southern and western Amazonia, but the June–July peak in precipitation is completely missed by all model simulations over northern Amazonia (Boa Vista). Rather, the models exhibit double peaks in precipitation, in May–June and October–November, evidently a result of the northward and southward migra-

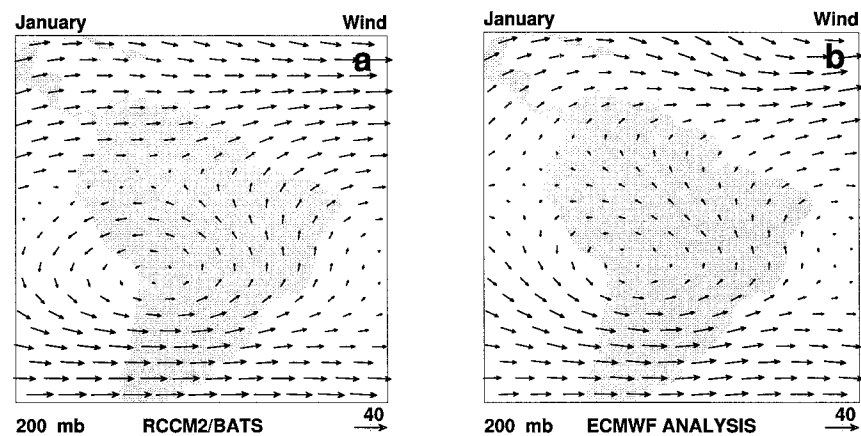


FIG. 4. Comparison of the ensemble-averaged January 200-hPa wind field (a) simulated by the RCM2-BATS model and (b) that from the observationally derived ECMWF analysis. The length of the arrows on the bottom right of each figure represents a wind speed of  $40 \text{ m s}^{-1}$ .

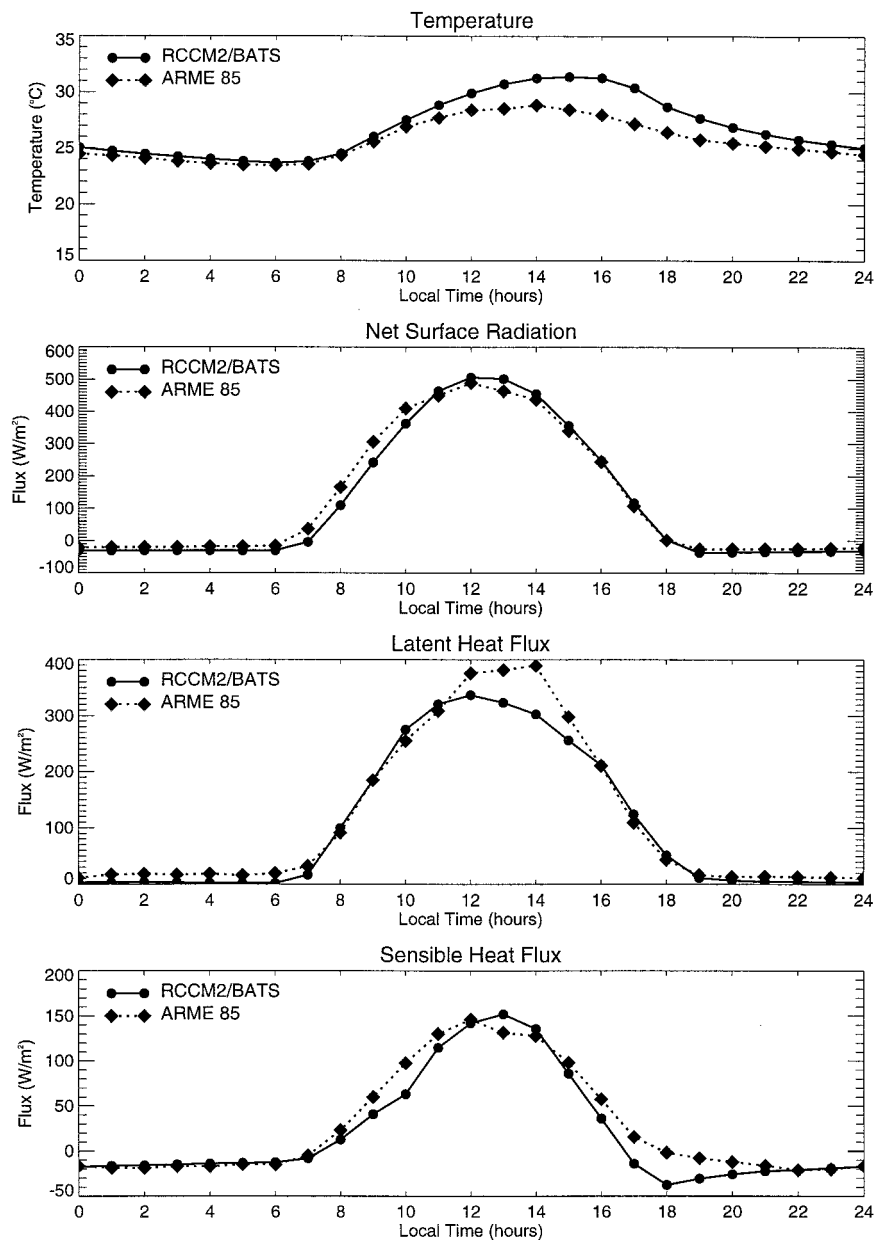


FIG. 5. Comparison of the model-simulated diurnal cycle of near-surface air temperature, net surface radiation, and latent and sensible heat fluxes with those measured during the ARME field campaign during April 1985.

tion of the model-simulated ITCZ during the year, as similarly found by Nobre et al. (1991). Observations of precipitation and OLR over northern South America (not shown) suggest that in reality the displacement of the maximum convective region does not follow a simple north-south path but has a more northwest to southeast track in the transition period from the Gulf of Panama to the Amazon region (Horel et al. 1989), giving in a single wet period in some parts of northern Amazonia.

#### *b. Atmospheric circulation*

The tropospheric circulation over the tropical South American sector is evaluated using wind data from the World Meteorological Organization (WMO)-European Centre for Medium-Range Weather Forecasts (ECMWF) archive (Trenberth 1992), averaged over the period 1985-92. The pressure levels of 850 and 200 hPa represent the low-level wind flow as affected by the topographic features of the continent and the high-

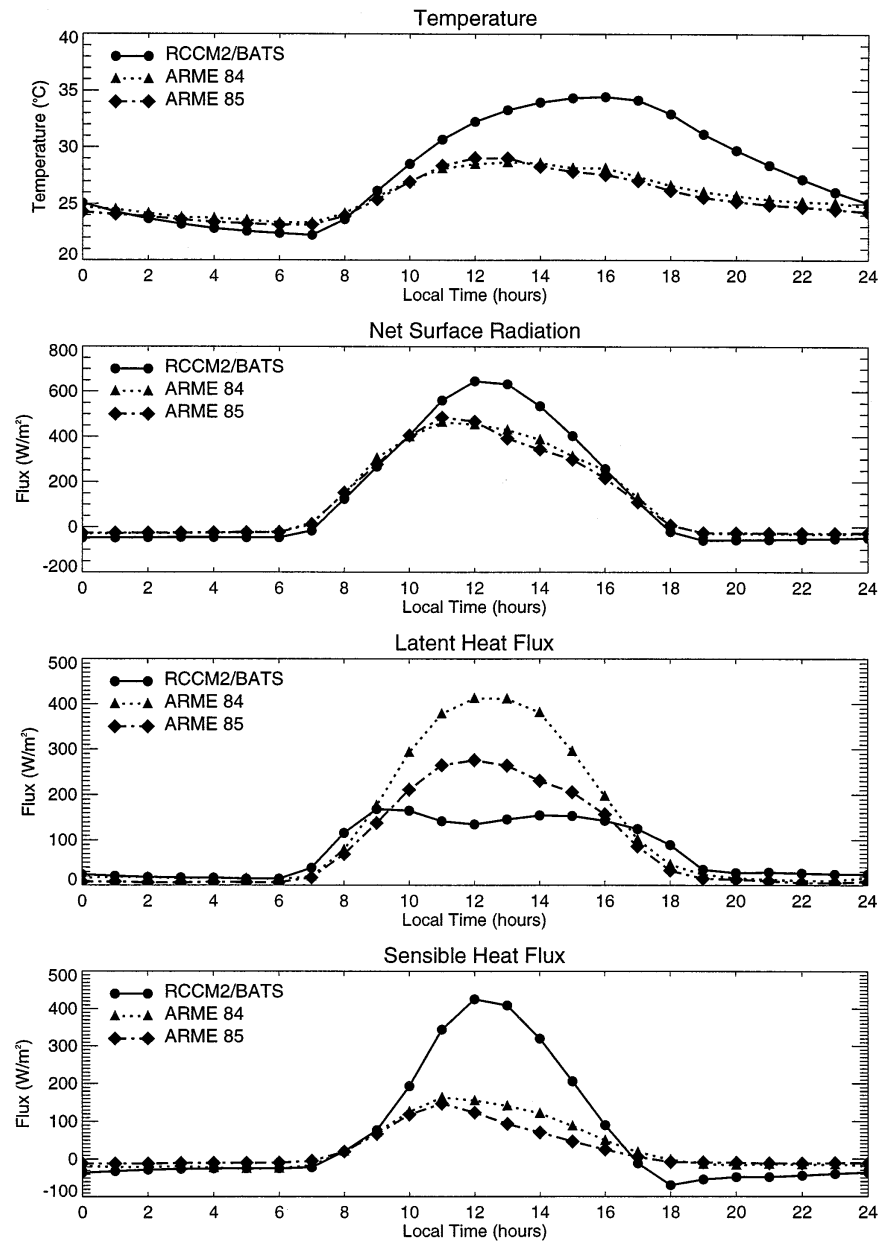


FIG. 6. Comparison of the model-simulated diurnal cycle of near-surface air temperature, net surface radiation, and latent and sensible heat fluxes with those measured during the ARME field campaign during August 1984 and 1985.

level tropospheric circulation as determined by the convective activity in Amazonia. The upper-tropospheric circulation is very similar in all models, apparently determined by the strength and position of the area of intense deep convection, so only the RCCM2-BATS simulation is considered further. Figure 3 compares the wind field at the 850-hPa surface for the January ensemble-averaged model simulation with the ECMWF analysis. Figure 3b displays the climatological low-level circulation with the two midlatitude anticyclones over the Pacific and Atlantic Oceans and the intense easterlies

over the northern South American coast. The low-level flow entering the western Amazon Basin region becomes northeasterly and finally northerly, perhaps turned by the Andes Mountains. The model simulation (Fig. 3a) captures this pattern very well, except for the intensity of the low-level flow over northeastern Brazil, where weak easterlies are observed, versus the stronger simulated easterlies (on the order of  $10 \text{ m s}^{-1}$ ).

Figure 4 compares the features of the upper-tropospheric circulation, including the Bolivian high centered over southern Peru and Bolivia and the downstream

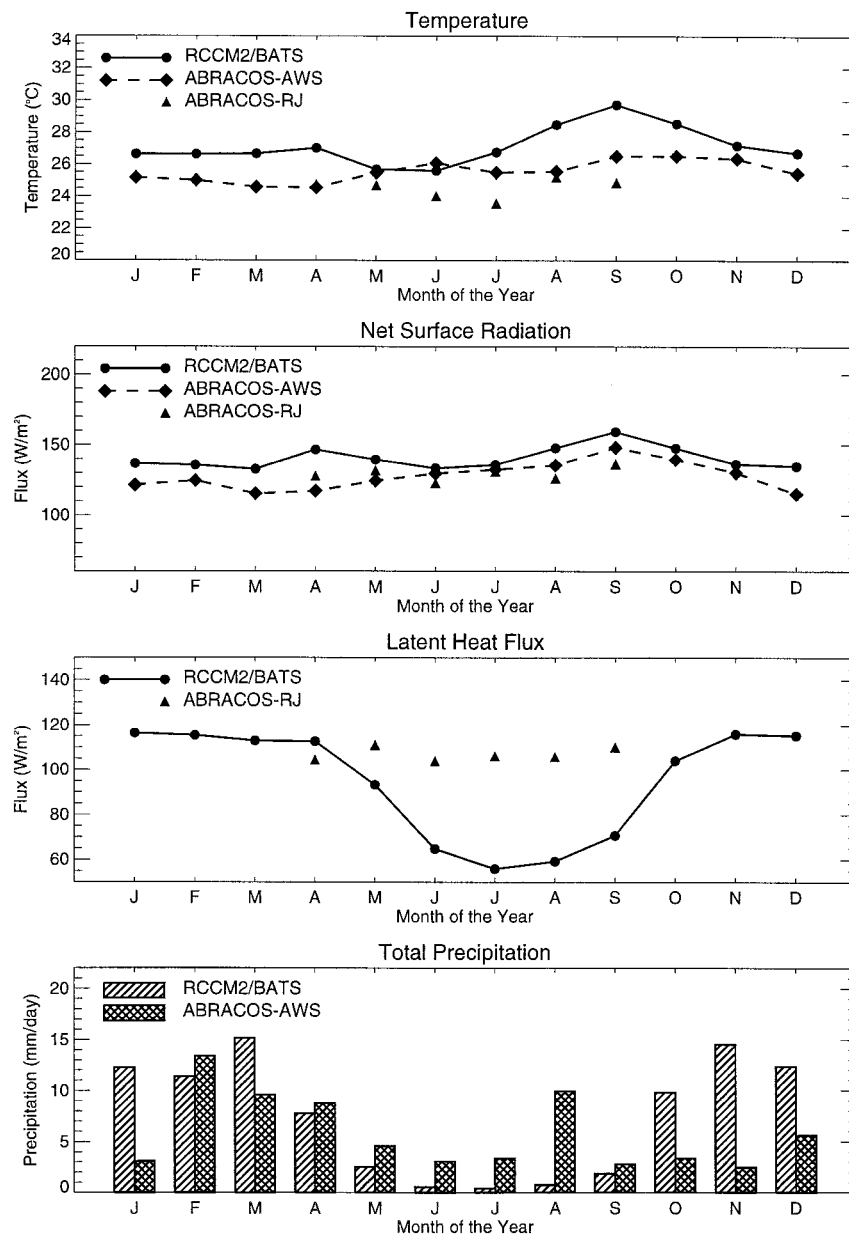


FIG. 7. Comparison of model-simulated, ensemble-averaged near-surface air temperature, net surface radiation, latent heat flux, and precipitation with observed monthly averages estimated from measurements taken during the ABRACOS field campaign. Model data is averaged over a  $8.4^\circ$  area centered at  $7^\circ\text{S}$ ,  $59^\circ\text{W}$ . ABRACOS-AWS estimates are derived from AWS measurements at Reserva Duke, while ABRACOS-RJ are derived from micrometeorological measurements at Reserva Jaru.

trough centered over the easternmost coast of Brazil (Horel et al. 1989). The model simulation (Fig. 4a) is remarkably similar to the ECMWF analysis (Fig. 4b) at this level, except for the Northern Hemisphere westerlies. The model simulates a band of westerlies (with a magnitude of approximately  $20 \text{ m s}^{-1}$ ) extending from the Gulf of Panama into the northern part of the Amazon Basin, whereas the ECMWF analysis shows this westerly jet to be located farther north over the Caribbean.

### c. Near-surface climate

Several field campaigns provide an excellent database for model validation of the near-surface climate. Model simulations of the diurnal cycle of near-surface temperature and heat fluxes are assessed using micrometeorological data collected during the Amazon Region Micrometeorological Experiment (ARME) from the early 1980s at the Reserva Duke, near the city of Manaus,

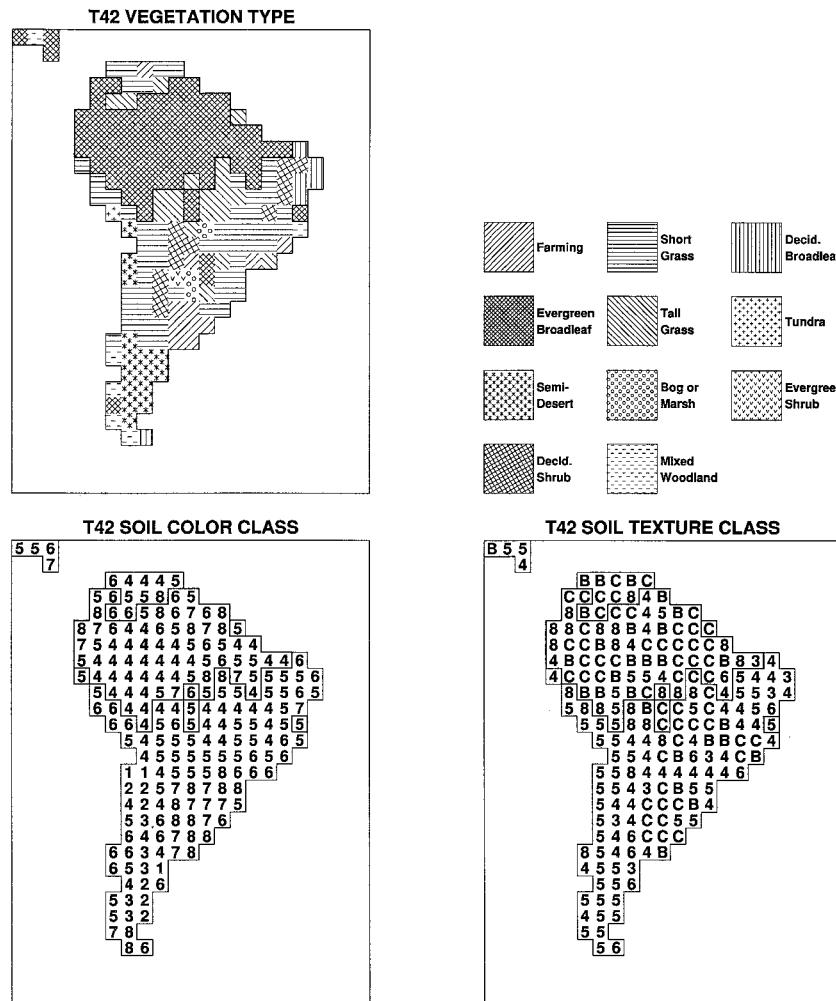


FIG. 8. T42 vegetation types and soil color [from light (1) to dark (8)] and texture [from sand (1) to clay (C)] classes for South America. Soil texture classes A = 10, B = 11, and C = 12. The evergreen broadleaf vegetation type was replaced by degraded grassland in the deforestation experiments.

in central Amazonia. Data from three intensive field campaign periods were used: August 1984 (ARME84), and April and August 1985 (ARME85). These three months were selected because of their good data coverage of hourly latent and sensible heat fluxes during both the month and the day (at least a third of the days of the month with at least 12 observations during the day). The second dataset corresponds to automatic weather station (AWS) observations and micrometeorological measurements taken during the Anglo-Brazilian Amazonian Climate Observational Study (ABRACOS). For comparisons against model simulated data, we have used AWS measurements for Reserva Duke ("RD", 2°57'S, 59°57'W) and Reserva Jaru ("RJ", 10°05'S, 61°55'W) located in the Brazilian state of Rondônia.

Figures 5 and 6 compare the observed diurnal cycle of surface temperature and surface fluxes with those

simulated by RCM2-BATS at a single grid point closest to the Reserva Duke site. The model data are hourly averages from the seventh year (year 12) of the 10-yr control simulation. At the end of the wet season (April, Fig. 5) the simulated net surface radiation and surface fluxes are in close agreement with their observed counterparts in both phase and amplitude. Latent heat fluxes are slightly underestimated (by less than 100 W m<sup>-2</sup>) in the early afternoon. Simulated near-surface temperatures are within 1°C of those observed during the nighttime and about 3–4°C warmer during the daytime. Some of this disagreement may be an artifact of differences in measurement level between the observed and simulated temperatures. ARME temperatures were measured at a height of approximately 45 m, slightly above the forest canopy, while first model level air temperatures refer to a height of approximately 70 m.

During the peak of the dry season in Amazonia (Au-

TABLE 3. BATS surface parameters for tropical forest (class 6) and degraded grassland (class 20) vegetation types.

Factor	Tropical forest	Degraded grassland
Maximum vegetation cover	0.9	0.8**
Vegetation roughness length (m)	2.0	0.05**
Rooting ratio	0.8	0.5**
Vegetation albedo < 0.7 μm	0.04	0.08*
Vegetation albedo ≥ 0.7 μm	0.2	0.3*
Minimum stomatal resistance (s m <sup>-1</sup> )	150	200**
Maximum leaf area index	6.0	6.0
Stem area index	2.0	2.0
Light sensitivity factor (m <sup>2</sup> W <sup>-1</sup> )	0.06	0.02**
Vegetation displacement height (m)	18.0	0.0**
Depth of upper soil layer (mm)	100	100
Depth of root zone (mm)	1500	1000
Depth of total soil layer (mm)	5000	5000

\* Changes included in the ALBEDO experiment.  
 \*\*Changes included in the ROUGH experiment.

gust, Fig. 6), RCCM2-BATS appears to substantially underestimate the latent heat flux during the daytime hours, although observed latent heat fluxes differ by as much as 100–150 W m<sup>-2</sup> between two consecutive years. These discrepancies are due in part to the excessive dryness of the model simulation during the Amazonian dry season. Figure 2 shows that the model simulates rainfall amounts of the order of 25 mm day<sup>-1</sup>, while Shuttleworth et al. (1991) indicate precipitation amounts of the order of 100 mm day<sup>-1</sup> in the 3 months prior to August 1984 and August 1985. Although BATS has adequate net surface radiation, the low precipitation limits the amount of water available in the soil for evapotranspiration. Furthermore, results from the ABRACOS field campaign summarized in Wright et al. (1996) suggest that root zone depths over Amazonia may be severely underestimated in the model. Their measurements show strong evidence at all forest sites for soil water extraction by deep roots (i.e., those that penetrate below depths of 3.5 m), while the BATS evergreen deciduous tree vegetation type assumes a root zone depth of only 1.5 m. Temperatures are too warm by as much as 8°C during the daytime hours, which is also a consequence of the severe underestimation of evaporation rates.

Small evaporation rates occur in RCCM2-BATS during the dry season from the central to the southern Amazon. Figure 7 displays the seasonal cycle of air temperature, net surface radiation, latent heat flux, and precipitation averaged over a 8.4° area centered at 7°S, 59°W. These model evaporation rates are consistently smaller than ABRACOS-derived estimates of monthly near-surface parameters for the period from May to September, as also are the rainfall rates. The simulation of net surface radiation, however, matches the observations during most of the year and is a considerable improvement over previous CCM simulations (Dickinson and Henderson-Sellers 1988; Dickinson and Kennedy 1992).

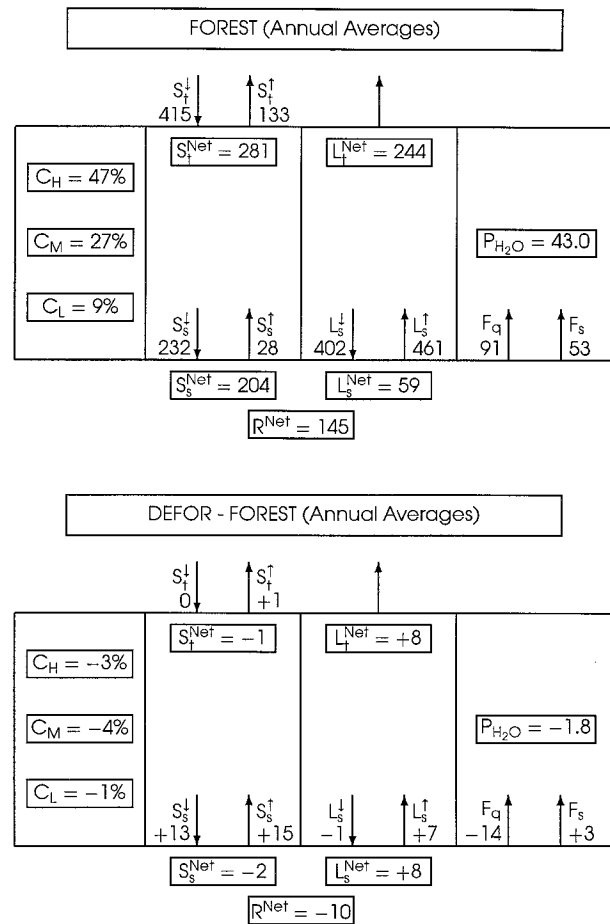


FIG. 9. Annual surface and top-of-the-atmosphere energy budgets for the FOREST simulation and the difference between the DEFOR experiment and the control averaged over the Amazon region. Units are in W m<sup>-2</sup> or otherwise noted. Symbols are as follows: C<sub>L</sub>, C<sub>M</sub>, and C<sub>H</sub> are low, middle, and high cloud fractions (in percentage), respectively; S<sub>s</sub><sup>↓</sup>, S<sub>s</sub><sup>↑</sup>, and S<sub>s</sub><sup>Net</sup> are downward, upward, and net downward shortwave fluxes at surface, respectively; L<sub>s</sub><sup>↓</sup>, L<sub>s</sub><sup>↑</sup>, and L<sub>s</sub><sup>Net</sup> are downward, upward, and net upward longwave fluxes at surface, respectively; R<sup>Net</sup> is the net radiation into the surface; S<sub>t</sub><sup>↓</sup>, S<sub>t</sub><sup>↑</sup>, and S<sub>t</sub><sup>Net</sup> are downward, upward, and net downward shortwave fluxes at top, respectively; L<sub>s</sub><sup>Net</sup> is the outgoing longwave radiation at top; P<sub>H<sub>2</sub>O</sub> is the precipitable water (in mm); and F<sub>q</sub> and F<sub>s</sub> are the surface upward latent and sensible heat fluxes.

#### 4. Model sensitivity to tropical deforestation

The model used to represent tropical deforestation (simulation labeled “DEFOR” in Table 2) has a complete replacement of the tropical forest vegetation (Evergreen Broadleaf Trees class in BATS1e) by a new vegetation class composed of ranchland or Degraded Grassland over Amazonia. The deforested area is approximately 6.7 × 10<sup>6</sup> km<sup>2</sup>, about two-thirds of the total area of Brazil, and is located in the northern part of South America as indicated in Fig. 8. Table 3 presents the BATS parameters for both Tropical Forest and Degraded Grassland vegetation types, largely the same as those used by Dickinson and Henderson-Sellers (1988)

TABLE 4. Annually averaged climatic changes over Amazonia.

Variable (units)	FOREST	DEFOR—FOREST	ALBEDO—FOREST	ROUGH—FOREST
Precipitation (mm)	2186	-363	-302	-128
Evaporation (mm)	972	-149	-97	-105
Moisture convergence (P—E; mm)	1214	-214	-205	-23
Total runoff (mm day <sup>-1</sup> )	2.8	-0.5	-0.5	-0.0
Surface runoff (mm day <sup>-1</sup> )	2.2	-0.2	-0.5	-0.1
Available root zone soil moisture (%)	64.9	-10.0	-15.3	-2.9
Surface air temperature (°C)	27.3	+1.0	+0.1	+1.2
Maximum temperature (°C)	34.0	+1.9	+0.1	+2.2
Minimum temperature (°C)	22.1	+0.4	+0.1	+0.6

and Dickinson and Kennedy (1992). Besides changes to some vegetation parameters, the soil texture class is increased by 2 (thus increasing soil porosity and decreasing soil saturated hydraulic conductivity), and the soil color class is reduced by 2 (thus increasing its albedo by 2%) over the deforested area (Fig. 8). Of these changes, those in vegetation albedo and roughness are

believed to be the most important in simulating the climate sensitivity to tropical deforestation.

The DEFOR simulation was started from initial conditions from the middle of June of the third year (year 7) of the RCCM2-BATS simulation and was integrated for 8.5 yr. The first 6 months of this simulation were not used in the analysis that follows.

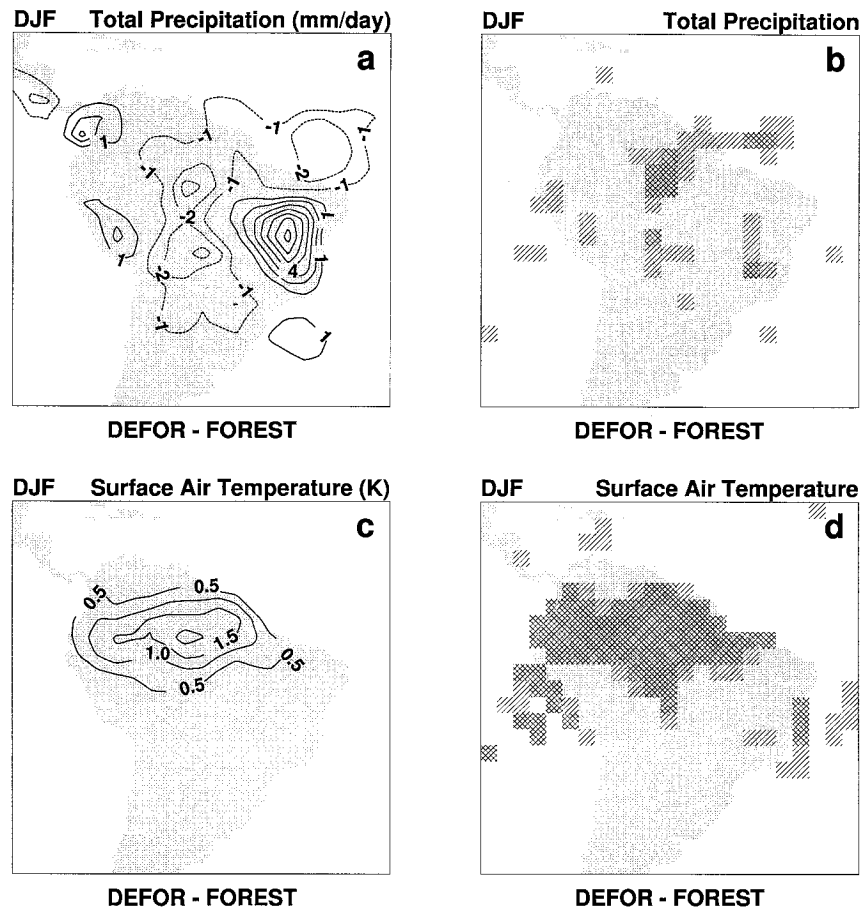


FIG. 10. DJF changes (DEFOR - FOREST) in (a) precipitation (mm day<sup>-1</sup>), (c) surface air temperature (°C), (e) evaporation (mm day<sup>-1</sup>), and (g) ratio of root zone available soil moisture (%) for the South American continent. (b), (d), (f), and (h) Respective Student's *t*-tests at the 95% (light hatch) and 99% (dark hatch) significance levels.

*a. Annual local response to deforestation*

The annual response to tropical deforestation is examined over a rectangular box (extending from 11.2°S to 2.8°N in latitude and from 71.7° to 52.0°W in longitude) contained within the deforested region and roughly corresponding to that used in previous deforestation studies. Figure 9a presents the annually averaged surface and top-of-the-atmosphere (TOA) energy budget averaged over this box for the control (RCCM2-BATS, named FOREST from this point on) simulation. The differences between DEFOR and the control experiment are presented in Fig. 9b. Table 4 concentrates on the hydrological cycle quantities and the surface temperatures for the control and experiment minus control, annually averaged over the same area box.

The albedo increase imposed in the DEFOR simulation by itself should have resulted in a large decrease in net shortwave radiation at the surface, that is, 15 W m<sup>-2</sup> (Dickinson and Kennedy 1992). However, a decrease in cloud cover fraction, especially in middle (-4%) and high (-3%) clouds, allows for an increase in downward solar radiation (+13 W m<sup>-2</sup>), which largely cancels the effect of the albedo change, so that the net decrease in net downward solar radiation at the sur-

face is only 2 W m<sup>-2</sup>. The changes in the net upward longwave flux (+8 W m<sup>-2</sup>) are dominated by an increase in upward longwave flux of 7 W m<sup>-2</sup> resulting from the increase in surface temperature (Table 4). The changes in cloud cover fraction and precipitable water (reduction of 1.8 mm) have little effect on the downward longwave flux (-1 W m<sup>-2</sup>). The solar and longwave changes together imply a decrease of 10 W m<sup>-2</sup> in the net radiation at the surface, and this is dominated by the longwave part of the surface energy budget. The TOA changes are also dominated by the changes in outgoing longwave radiation with an increase of 8 W m<sup>-2</sup> over the deforested area. The largest relative impact of the deforestation process in the surface energy budget is in the latent heat flux, with a reduction of 14 W m<sup>-2</sup> (-15%). In addition, the sensible heat flux increases by 3 W m<sup>-2</sup>, and correspondingly, the Bowen ratio changes from 0.58 in the forest to 0.73 in the degraded grassland environment.

Total annual precipitation shows a modest annual decrease of 363 mm over the deforested box area. This value is somewhat smaller than that simulated with previous versions of CCM1 coupled to BATS, that is, -511 mm in Dickinson and Kennedy (1992), and -588 mm

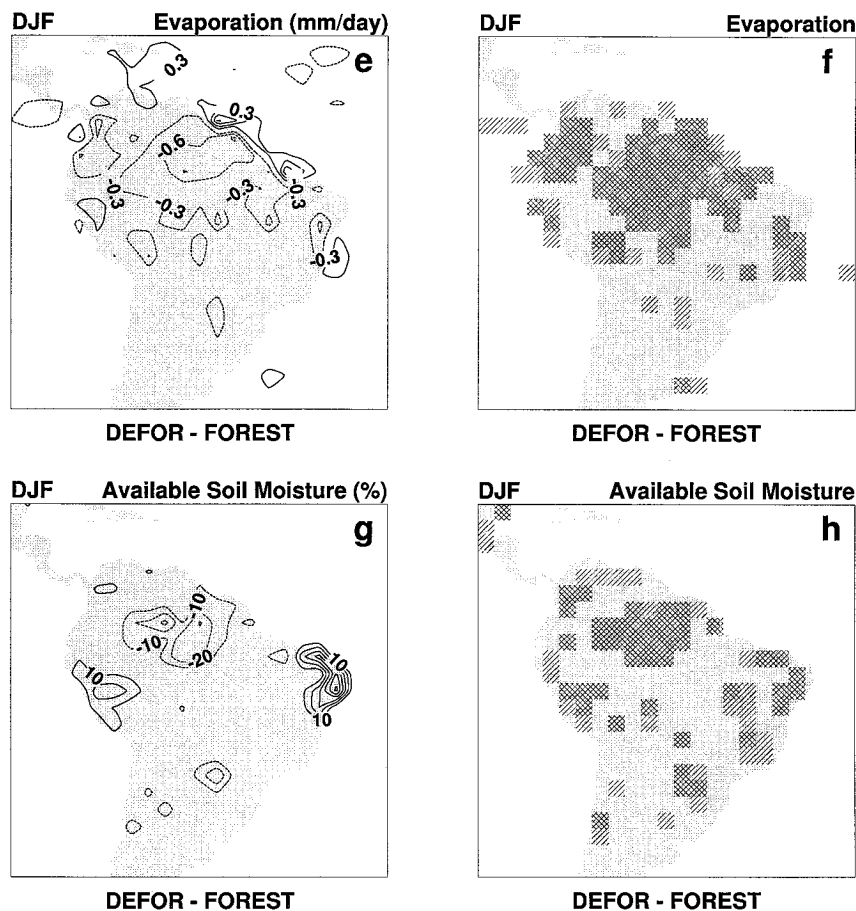


FIG. 10. (Continued)

and  $-437$  mm in Henderson-Sellers et al. (1993) and McGuffie et al. (1995), respectively. The last two studies used smaller changes in roughness length (Table 1). Annual evaporation decreases are also relatively small ( $-149$  mm) compared to those found in the previous deforestation experiments; that is, they are smaller than the decrease in precipitation, or equivalently, there is a decrease in the convergence of moisture into this region. Soil moisture changes show an interesting behavior. While surface and total soil water show slight increases ( $+0.9$  mm and  $+0.7$  cm, respectively), the root zone available soil moisture (defined as the ratio of excess moisture in soil above wilting point to the field capacity of the root zone soil layer) shows a decrease of approximately 10% over the deforested area, largely a result of the change in root zone depth and soil texture.

There is considerable spatial variability in the deforestation minus control differences, especially in the precipitation (see next section). Consequently, the spatial location of the averaging box may strongly affect the inferred statistics.

#### *b. Seasonal regional response*

Figure 10 displays the December–February (DJF) regional changes in precipitation, surface air temperature, evaporation, and fraction of available root zone soil moisture that result from deforestation in the RCCM2–BATS simulation. Next to each difference map (DEFOR – FOREST) are shown the Student's *t*-test contours of the statistical significance of these differences at the 95% and 99% levels (computed using a two-sample *t* test with 16 degrees of freedom).

The changes in precipitation (Fig. 10a) display an interesting bimodal pattern with decreases over central Amazonia extending east and north over the northern coast of South America and south into central Brazil and northern Argentina, and large increases concentrated over northeastern Brazil. These changes are only marginally significant, because of the large interannual variability in the precipitation field in this region (even with fixed seasonal SSTs). Figure 10c shows a large region of temperature increase of over  $2^{\circ}\text{C}$ , roughly overlapping the deforested area, a direct result of the decrease in roughness length and in evaporative cooling by the latent heat flux from the surface (Fig. 10e). No bimodal pattern is seen in the temperature and evaporation fields because of compensating changes in net radiation and soil moisture over northeastern Brazil. Additionally Fig. 10g shows that a decrease in the fraction of soil moisture available for plants.

Along the northeastern coast of South America, the coastline divides decreases in evaporation over land from increases over the adjacent Atlantic Ocean. The changes in roughness length over land act to increase the boundary layer winds over the deforested area, by about  $3\text{ m s}^{-1}$  at the first model level above the surface. This aerodynamic effect extends farther out over the

adjacent ocean, where drag coefficients are fixed and soil moisture content is not a limiting factor, and there causes an increase in latent heat flux. Over land, however, wind speed increases are not large enough to compensate for the decrease in the drag coefficient.

#### **5. Albedo versus roughness sensitivity**

The deforestation simulation, as described in the previous section, combines the effects of both albedo increase and surface roughness decrease on the climate of South America, as expected for deforestation. However, to better understand the processes involved and how they respond to deforestation changes, we examine separate sensitivity simulations of the effects of albedo and surface roughness. For this, two additional 5-yr simulations were performed using the RCCM2–BATS model. First (ALBEDO in Table 2), only vegetation albedos and soil color classes were changed as in DEFOR, corresponding to the radiative forcing of the deforestation process. Second (ROUGH in Table 2), only the plant physiological properties (e.g., vegetation cover fraction, roughness length, vegetation displacement height) were changed, corresponding mainly to an aerodynamic forcing of the deforestation process. All BATS parameters modified in one or another of these simulations are listed in Table 3. Neither simulation contains the changes to soil texture and soil depth introduced in DEFOR. Both were started from the same initial conditions as DEFOR, with again the first 6.5 months of integration discarded.

Besides the decrease in roughness length, the ROUGH simulation also incorporates changes to other BATS ecological parameters. The sensitivity of BATS evapotranspiration and temperature to changes in these parameters are indicated by several past studies that used multiple integrations of off-line versions of BATS. Henderson-Sellers (1992) showed that BATS is sensitive to a relatively small number of its parameters, which in decreasing order of importance are the vegetation roughness length, the vegetation albedos, and the light-sensitivity factor. However, the importance of the light-sensitivity factor decreases when it is considered over grass instead of tall vegetation. Gao et al. (1996) determined that BATS is most sensitive to fractional vegetation cover and roughness length. The decrease in vegetation cover fraction may accentuate the increase in surface temperatures, but its effect is probably much smaller than that of the reduced roughness effect.

#### *a. Annual local response*

Figure 11 shows how the surface and TOA energy budgets for ALBEDO and ROUGH differ from the control simulation. Surface radiation budget changes are especially pronounced. Cloud cover changes most in ALBEDO and results in increases in surface downward solar flux in both simulations ( $+9$  and  $+5\text{ W m}^{-2}$  in ALBEDO and ROUGH, respectively). Solar surface net

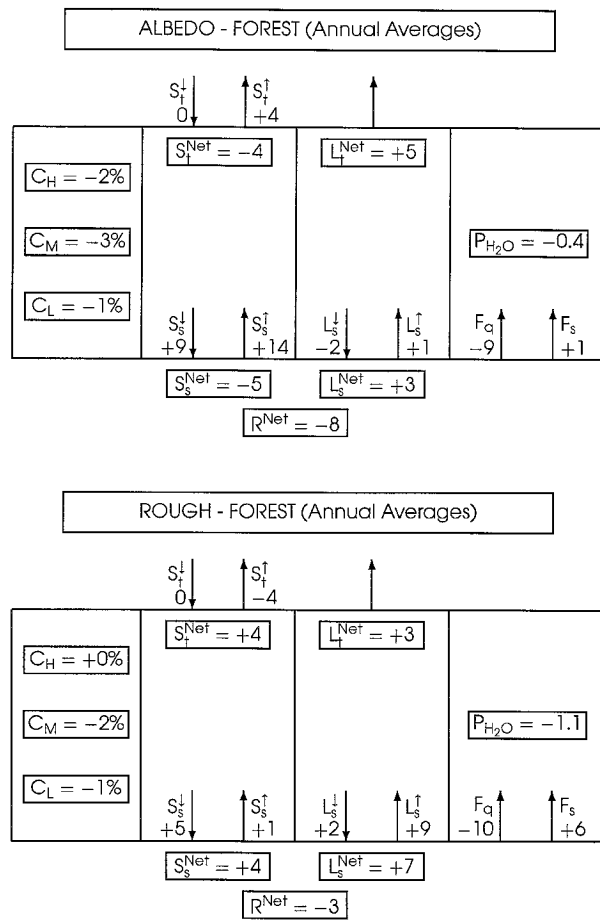


FIG. 11. Annual surface and top-of-the-atmosphere energy budget differences (experiment-FOREST) for ALBEDO and ROUGH averaged over the Amazon region. Symbols as in Fig. 9.

radiation decreases ( $-5 \text{ W m}^{-2}$ ) in ALBEDO from the imposed increase in albedo, but in ROUGH, this parameter actually increases by  $4 \text{ W m}^{-2}$ . The downward longwave flux changes nonlinearly in response to changes in high cloud cover and atmospheric boundary layer temperatures. In both cases, the increase in atmospheric boundary layer temperatures is not large enough to compensate for the effect of the reduction in high-level clouds, and hence downward longwave radiation at the surface is reduced. In ROUGH, however, high-level clouds increase slightly (especially during the Amazonian wet season), which, with the boundary layer temperature increases, increases downward longwave flux at the surface. Increases in upward longwave fluxes simply result from the increased surface temperatures.

The changes in surface net radiation in ALBEDO ( $-8 \text{ W m}^{-2}$ ) and ROUGH ( $-3 \text{ W m}^{-2}$ ) appear to add almost linearly to that of the DEFOR simulation, which has a  $-10 \text{ W m}^{-2}$  change in surface net radiation. In ALBEDO, the decrease in net surface radiation results directly in a latent heat flux reduction of  $9 \text{ W m}^{-2}$ , whereas the sensible heat flux change is too small to be signif-

icant. In ROUGH, the decreased roughness, hence drag coefficient, also decreases the surface evaporation, but this is largely balanced by an increase in sensible heat flux, which is consistent with the large increase in surface temperatures. Consequently, the Bowen ratio changes from 0.58 in FOREST to 0.66 and 0.73 in ALBEDO and ROUGH, respectively, compared to 0.73 in DEFOR. The sensible and latent heat fluxes for the individual sensitivity studies do not add linearly to the results from DEFOR.

The changes to the annually averaged hydrological cycle and surface temperatures for ALBEDO and ROUGH are summarized in Table 4. Both show decreases in precipitation ( $-302$  and  $-128 \text{ mm yr}^{-1}$ , respectively) and surface runoff ( $-0.5$  and  $-0.1 \text{ mm day}^{-1}$ , respectively). However, the ROUGH simulation shows a negligible decrease in moisture convergence, and during the Amazonian wet season, it displays an increase in precipitation. Together with the general decrease in evaporation, this increase results in an increase in moisture convergence over the deforested region. As expected, ALBEDO shows no significant changes in surface temperature, but large changes ( $+1.2^\circ\text{C}$  in the daily average of surface air temperature and  $+2.2^\circ\text{C}$  in its maximum) occur in the ROUGH simulation. In all simulations the soil has dried relative to the control, especially in ALBEDO, which shows a decrease of 15% in the root zone available soil moisture.

To complete this picture, we examine of the annual cycle of these changes. Figure 12 shows the ensemble-averaged annual cycle of surface air temperature, precipitation, evaporation, and root zone available soil moisture. It also quantifies the significance of these changes by displaying the interannual variability of the control monthly averages. Surface air temperature increases, as expected, in ROUGH throughout the year, but the changes in DEFOR are significant only for the period from September to April. With the large interannual variability of precipitation, deforestation-induced changes are significant only at most during some months of the year (March of all deforestation experiments and September for DEFOR and ROUGH). The significant evaporation changes, occurring throughout the year, are especially large at the end of the dry season and at the beginning of the wet season (September–November), suggesting that the onset of the wet season is somewhat delayed in ALBEDO and DEFOR. Changes in available soil moisture in the root zone layer during the Amazonian dry season follow changes in net water input from the previous wet season. In ALBEDO, precipitation decreases most during March and April, which, with the smaller decreases in evaporation and runoff (not shown), determine very low soil moisture amounts within the root zone layer.

#### b. Regional response to albedo and roughness changes

Figure 13 shows the DJF regional changes in precipitation and evaporation induced by the changes in albedo

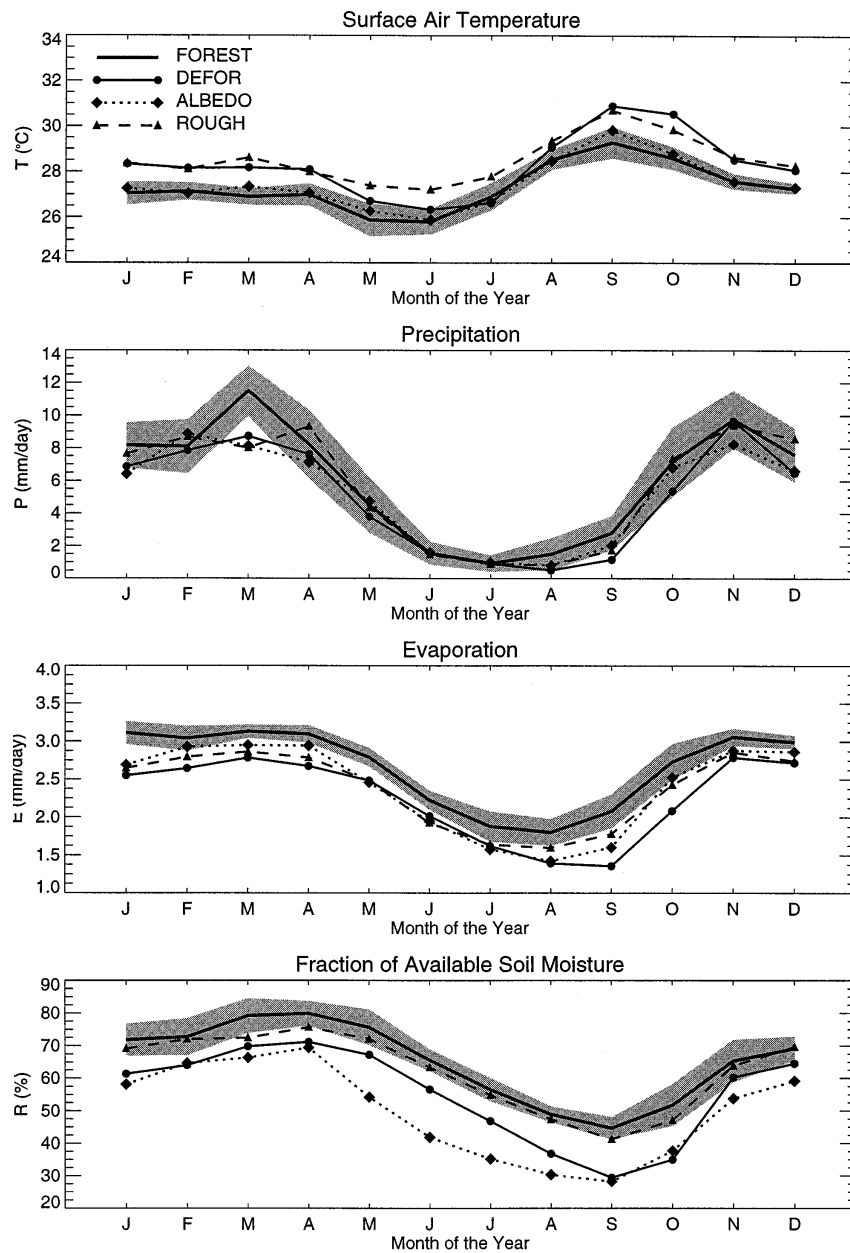


FIG. 12. Monthly values of area-averaged surface air temperature ( $^{\circ}\text{C}$ ), precipitation ( $\text{mm day}^{-1}$ ), evaporation ( $\text{mm day}^{-1}$ ), and ratio of root zone available soil moisture (%) for the control simulation (FOREST) and the three deforestation experiments (DEFOR, ALBEDO, and ROUGH). The shaded area in each time series is FOREST values plus or minus one standard deviation of the ensemble monthly means.

alone (ALBEDO — FOREST). As in DEFOR, a bimodal pattern of precipitation changes emerges. The area of maximum precipitation shifts eastward producing the pattern shown in Fig. 13a: large differences in precipitation over central Brazil, with a maximum decrease of about  $4 \text{ mm day}^{-1}$ , and large increases over northeast Brazil (up to  $5 \text{ mm day}^{-1}$ ). However, only the central portion of these areas is statistically significant (Fig. 13b). Evaporation (Fig. 13c) decreases over most

of northern South America, with a maximum decrease over central Amazonia and small areas of significant increase over the central Andes and the northeast tip of the continent.

The changes introduced in ROUGH induce a very different pattern in the precipitation field. Figure 14a shows increases in precipitation (about  $1 \text{ mm day}^{-1}$ ) over southern Amazonia with small decreases along the northern coast of South America. This difference pattern

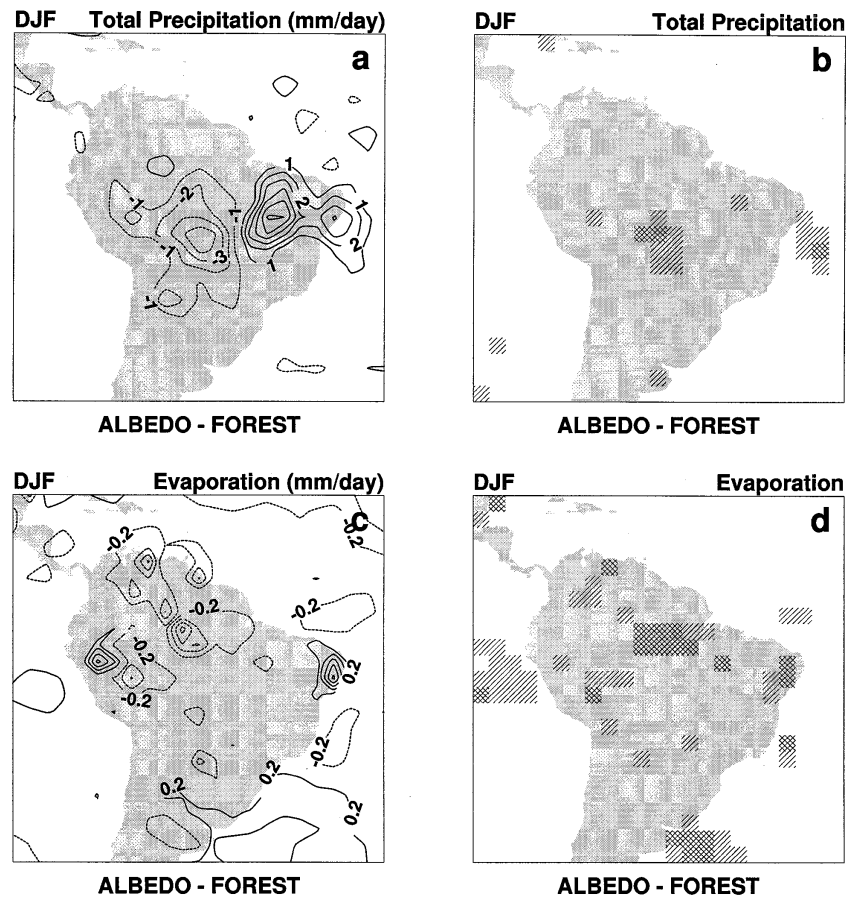


FIG. 13. DJF changes (ALBEDO-FOREST) in (a) precipitation ( $\text{mm day}^{-1}$ ) and (c) evaporation ( $\text{mm day}^{-1}$ ) for the South American continent. (b) and (d) Respective Student's *t*-tests at the 95% (light hatch) and 99% (dark hatch) significance levels.

suggests a southward shift of the precipitation field, but with limited significance. The changes in evaporation overlap the deforested area and display the previously mentioned pattern over land and ocean along the coastline.

Changes in the precipitation pattern over Amazonia are intrinsically related to changes in its supply of moisture. Hence, we have computed the vertically integrated water vapor flux and water vapor flux convergence, as written in

$$\frac{\partial \bar{Q}}{\partial t} = -\frac{1}{g\rho_w} \int_0^{p_s} \nabla \cdot \bar{q}\bar{\mathbf{V}} dp + \bar{E} - \bar{P}, \quad (1)$$

where  $Q$  is vertically integrated atmospheric water vapor content;  $g$  is acceleration of gravity;  $\rho_w$  is density of water;  $p_s$  is surface pressure;  $\nabla$  is the horizontal divergence operator;  $q$  is water vapor specific humidity;  $\mathbf{V}$  is horizontal wind velocity;  $E$  and  $P$  are evaporation and precipitation rates, respectively; and the overbar indicates climatological means. The integral term giving the moisture convergence ( $C$ ) can be divided into its time-mean and transient components:

$$\bar{C} = -\frac{1}{g\rho_w} \int_0^{p_s} \nabla \cdot \bar{q}\bar{\mathbf{V}} dp - \frac{1}{g\rho_w} \int_0^{p_s} \nabla \cdot \bar{q}'\bar{\mathbf{V}}' dp, \quad (2)$$

where the primes denote deviations from the 3-month climatological mean. Lenters and Cook (1995) have shown from GCM-derived atmospheric water budgets over South America that the Amazonian precipitation maximum is primarily associated with large-scale convergence (87% of the regional precipitation rate), with only a small fraction of water vapor transported by transient eddies (−18% of the regional precipitation rate). Following their findings, the quasi-steady moisture convergence term, which is the first integral in (2), is used as a proxy for moisture convergence over Amazonia. Seasonal (e.g., DJF) water vapor fluxes and moisture convergence fields are computed from specific humidity and wind fields initially averaged over each season for all available years and then averaged over these years to represent an ensemble-averaged seasonal value.

As expected, the horizontal pattern of the vertically integrated water vapor flux (Fig. 15a) for the DJF season is almost identical to that of the low-level wind field

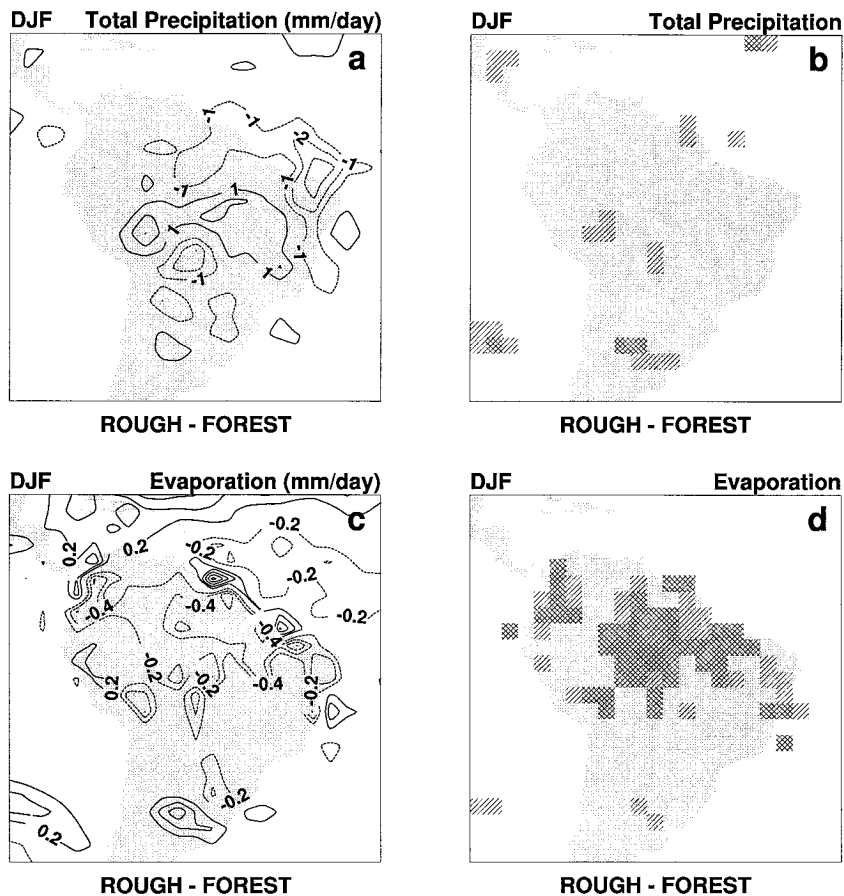


FIG. 14. DJF changes (ROUGH-FOREST) in (a) precipitation ( $\text{mm day}^{-1}$ ) and (c) evaporation ( $\text{mm day}^{-1}$ ) for the South American continent. (b) and (d) Respective Student's *t*-tests at the 95% (light hatch) and 99% (dark hatch) significance levels.

depicted in Fig. 3a for January. Evidently, the Southern Hemisphere summer circulation is maintained almost intact throughout the season and most of the moisture is transported by the low-level flow. This flow from the Atlantic Ocean penetrates the South American continent all along its northern coast, supplying moisture to the Amazonian convective activity, with some transported south into central Brazil and northern Argentina. The moisture convergence field in Fig. 15b closely resembles the precipitation distribution over this region, confirmation that most of the moisture transport over this region is provided by the large-scale moisture flow. Its maximum is associated with the counterclockwise turning of the northeasterly trade winds crossing South America and their convergence with the easterlies emanating from the South Atlantic high (Lenters and Cook 1995).

Figure 16 shows how moisture flux changes in the various deforestation experiments. The scale of the arrows in this figure is twice the scale of the arrows in Fig. 15b. In ALBEDO (Fig. 16b), the moisture flux changes within Amazonia are mainly westerly with a maximum magnitude of  $70 \text{ kg m}^{-1} \text{ s}^{-1}$ , suggesting a

reduction in the moisture flux in central Amazonia and, as a result, a reduction in the moisture convergence (about  $2 \text{ mm day}^{-1}$ ) and precipitation over this region. The changes in the low-level moisture flow also point to a displacement of the area of maximum convergence farther east, thus producing the changes in precipitation displayed in Fig. 13a. The precipitation is further reduced by the decrease in evaporation. The changes in the water vapor flux have a very different appearance in the ROUGH simulation (Fig. 16c). Easterly water vapor fluxes increase from the mouth of the Amazon River region to central Amazonia by about  $50 \text{ kg m}^{-1} \text{ s}^{-1}$ , a pattern that results in increased moisture convergence over most of southern Amazonia by as much as  $2 \text{ mm day}^{-1}$  and, hence, an increase in precipitation (Fig. 13b).

Figure 16a shows that the water vapor flux changes in DEFOR appear to combine the effects of increased albedo and reduced roughness length in some regions. Over western Amazonia, easterly water vapor fluxes increase while changes over eastern Amazonia are small, so that the water flux divergence increases over central Amazonia and convergence increases to the west and

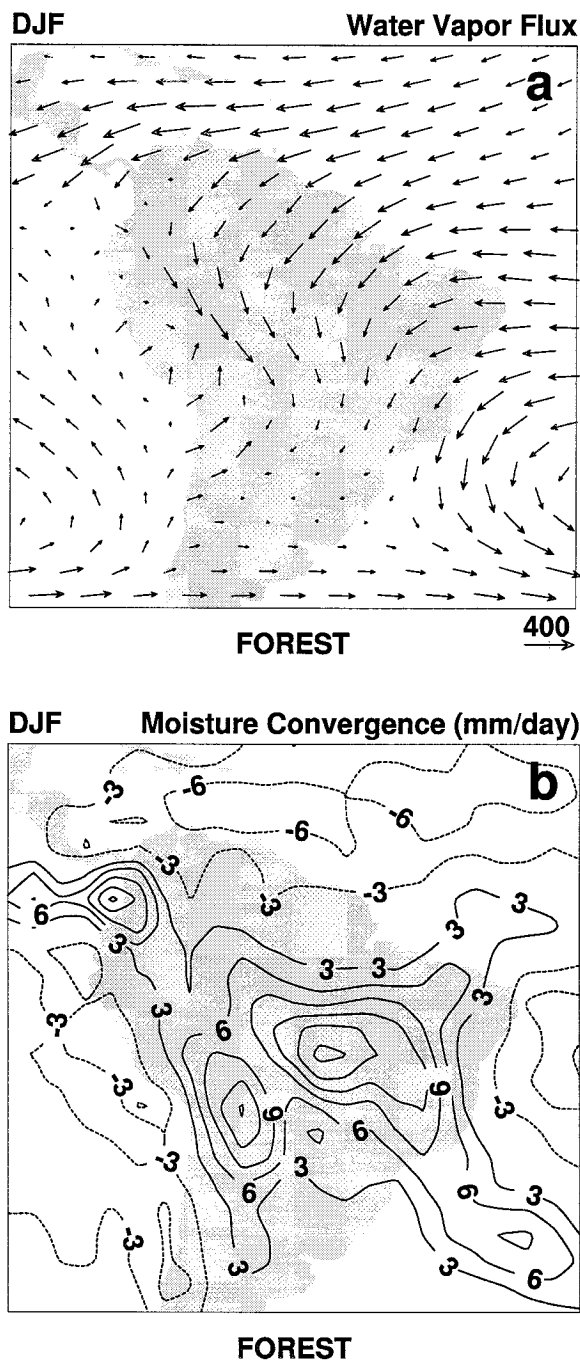


FIG. 15. DJF vertically integrated water vapor flux ( $\text{kg m}^{-1} \text{s}^{-1}$ ) (a) and vertically integrated moisture convergence ( $\text{mm day}^{-1}$ ) (b) for the control simulation (FOREST). The length of the arrow on the bottom right of (a) represents a water vapor flux of  $400 \text{ kg m}^{-1} \text{s}^{-1}$ .

east. The largest differences in water vapor flux are found over southeast Brazil, with an increase in its southern component. The moisture convergence changes suggest a northeasterly displacement of the region of intense convergence in the South Atlantic convergence zone.

## 6. Summary and conclusions

A multiyear simulation of the global climate using a revised version of the NCAR CCM2 model coupled to BATS (RCCM2-BATS) is evaluated against a variety of observational datasets for the tropical South American region. A realistic representation of the effects of tropical deforestation in GCMs requires a proper representation of the present climate by the control simulation. Therefore, the validation of the RCCM2-BATS model both globally (Hahmann et al. 1995) and regionally over northern South America is emphasized. Overall, the model simulation of the South American climate agrees closely with the available observational record.

Global and rain gauge precipitation climatologies are used to evaluate precipitation fields over South America, showing that the revisions to cloud optical properties introduced in the RCCM2-BATS model not only give radiative quantities but also a hydrological cycle in better agreement with observations. Both the climatological distribution and the annual cycle of precipitation improve. The model still overestimates the precipitation in the Amazonian wet season and underestimates it in the dry season. The model-simulated climatology of the low- and high-level wind fields over South America is remarkably similar to that observed in the ECMWF analyses.

The model-simulated annual and diurnal cycle of selected near-surface parameters are compared against several datasets from field campaigns executed in Amazonia. The net surface radiation and surface fluxes are in very close agreement during April, the period of transition from the wet to the dry seasons. During the dry season (August), RCCM2-BATS seriously underestimates the latent heat fluxes during the daytime hours, apparently a result of the excessive dryness of the model during this period and an underestimation of the model root zone depths over Amazonia. The net surface radiation is consistent with observations during most of the year and is a considerable improvement over that in previous CCM simulations.

The RCCM2-BATS model is then used to study the sensitivity of the Amazonian and South American climate to tropical deforestation. Three model simulations are conducted: DEFOR, where all surface parameters are changed according to previous deforestation experiments, and ALBEDO and ROUGH, where changes to individual deforestation parameters, mainly surface albedo and surface roughness, are tested. The DEFOR experiment shows an annual increase in surface temperature ( $+1^{\circ}\text{C}$ ) and a decrease in evaporation ( $-149 \text{ mm}$ ) and precipitation ( $-365 \text{ mm}$ ) in an area centered over the deforested region.

The moisture convergence and precipitation fields during the Amazonian wet season (December-February) change regionally by a shift in the areas of maximum precipitation rather than by an overall decrease

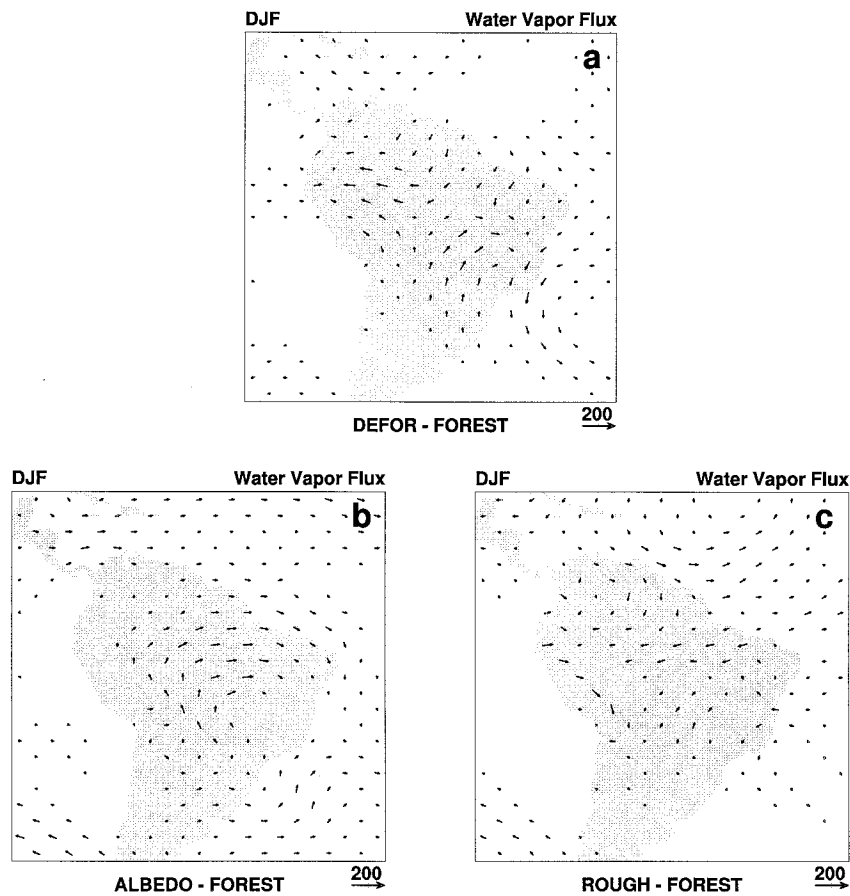


FIG. 16. DJF differences in vertically integrated water vapor flux ( $\text{kg m}^{-1} \text{s}^{-1}$ ) for (a) DEFOR - FOREST, (b) ALBEDO - FOREST, and (c) ROUGH - FOREST. The length of the arrow on the bottom right of each panel represents a water vapor flux of  $200 \text{ kg m}^{-1} \text{s}^{-1}$  (half the magnitude of the arrows in Fig. 15a).

over the deforested area. In DEFOR the maximum precipitation region is displaced southeastward, while in ALBEDO and ROUGH it is displaced eastward and southward, respectively. Dirmeyer and Shukla (1994) show a similar eastward shift in the precipitation field when rain forest albedos are increased by 0.06. GCM deforestation simulations by Manzi and Planton (1996) also display coherent shifts in precipitation, especially in their simulation with changes to the roughness length alone. However, the short duration of their sensitivity experiments (only 3 months) makes the significance of their results questionable. The observed shifts in precipitation appear to combine changes in the low-level circulation with a decrease in the efficiency of the recycling of water vapor within Amazonia as follows. In general, water vapor advected into Amazonia from the Atlantic Ocean precipitates near the Amazonian coast. Part of this water is reevaporated to the atmosphere and transported farther inland by the low-level wind field where it is precipitated and reevaporated. Estimates of basin-wide precipitation recycling range from 50% (Salati 1987) to 25% (Eltahir and Bras 1994). Decreases in

surface evaporation induced by the roughness decrease and albedo increase decrease the efficiency of the reevaporation of precipitated water (from transpiration or interception) and so increase precipitation near the moisture source and decrease it inland. Changes to the low-level circulation, however, are probably as important as the above mechanism.

The RCCM2-BATS model responds to tropical deforestation in a very pronounced bimodal pattern, especially in the precipitation field. Previous GCM deforestation studies have shown similar but less pronounced patterns (e.g., Dickinson and Henderson-Sellers 1988; Dirmeyer and Shukla 1994; Sud et al. 1996; Manzi and Planton 1996). This bimodality is problematical for the comparison of results among GCM deforestation studies, because it implies that the inferred area-averaged changes induced by deforestation depend on the position of the averaging box. Some of the area-averaged changes in precipitation and moisture convergence shown in Figs. 9 and 11 and Table 4 would change considerably or even reverse sign if the averaging box were displaced eastward.

Neither ALBEDO nor ROUGH simulations included the modifications of soil characteristics included in DEFOR. Pitman et al. (1993) considered such modification in a series of simulations using CCM1 coupled to BATS and found that the additional disturbances produced by brighter and finer soil gave a slight decrease in annual surface temperatures and small decreases in annual precipitation and evaporation, about one-fifth and one-third, respectively, smaller than those produced by their standard deforestation experiment (Table 1).

Several questions remain unanswered. What is the global impact of the deforestation changes? Global difference and significance plots of surface air temperature and precipitation (not shown) display very little sensitivity outside the South American sector, and no coherent pattern could be identified. Evidently, the simulations are still too short to reveal any such global connections. The work by Zhang et al. (1996) has extensively explored this subject. Also, what is the impact of climatological versus observed sea surface temperatures and their feedbacks? Koster and Suarez (1995) suggest that feedbacks associated with land-surface processes may amplify precipitation anomalies induced by SSTs and thus reduce or conceal the impacts of tropical deforestation on regional climate. Zeng et al. (1996), in considering deforestation in a mechanistic model coupled to a mixed layer ocean, suggest that a decrease in the SST gradient across the equatorial Atlantic Ocean, which might influence the climate over coastal Amazonia.

*Acknowledgments.* We thank Qing-Qiu Shao, Zong-Liang Yang, and Rong Fu for valuable discussions throughout the research. Thomas Dunne at the University of Washington provided the rainfall data for Amazonia. We also thank the NCAR SCD, founded by the National Science Foundation, and the MECCA Program of EPRI for supplying the required computational resources for the simulations reported here. We are grateful to Brian Auvine and Cas Sprout for editing the manuscript and to two anonymous reviewers who helped clarify our interpretation of the results. Funding for this study was provided by the National Science Foundation under Grant ATM-9419715 and by the Department of Energy under Grant DE-FG03-94ER61930.

#### REFERENCES

- Bastable, H. G., W. J. Shuttleworth, J. H. C. Gash, R. L. G. Dallara, G. Fisch, and C. A. Nobre, 1993: Observations of climate, albedo and surface radiation over cleared and undisturbed Amazonian forest. *Int. J. Climatol.*, **13**, 783–798.
- Bonan, G. B., 1994: Comparison of the land surface climatology of the National Center for Atmospheric Research Community Climate Model 2 at R15 and T42 resolutions. *J. Geophys. Res.*, **99**, 10 357–10 364.
- Briegleb, B. P., 1992: Delta-Eddington approximation for solar radiation in the NCAR Community Climate Model. *J. Geophys. Res.*, **97**, 7603–7612.
- Chu, P.-S., Z.-P. Yu, and S. Hastenrath, 1994: Detecting climate change concurrent with deforestation in the Amazon Basin: Which way has it gone? *Bull. Amer. Meteor. Soc.*, **75**, 579–583.
- Culf, A. D., G. Fisch, and M. G. Hodnett, 1995: The albedo of Amazonian forest and ranch land. *J. Climate*, **8**, 1544–1554.
- Dickinson, R. E., and A. Henderson-Sellers, 1988: Modelling tropical deforestation: A study of GCM land-surface parametrizations. *Quart. J. Roy. Meteor. Soc.*, **114**, 439–462.
- , and P. Kennedy, 1992: Impacts on regional climate of Amazon deforestation. *Geophys. Res. Lett.*, **19**, 1947–1950.
- , A. Henderson-Sellers, and P. J. Kennedy, 1993: Biosphere-Atmosphere Transfer Scheme (BATS) Version 1e as coupled to the NCAR Community Model. NCAR Tech. Note NCAR/TN-387+STR, 72 pp. [Available from National Center for Atmospheric Research, Boulder, CO 80307.]
- Dirmeyer, P. A., and J. Shukla, 1994: Albedo as a modulator of climate response to tropical deforestation. *J. Geophys. Res.*, **99**, 20 863–20 877.
- Eltahir, E. A. B., and R. L. Bras, 1994: Precipitation recycling in the Amazon Basin. *Quart. J. Roy. Meteor. Soc.*, **120**, 861–880.
- Gao, X., S. Sorooshian, and H. V. Gupta, 1996: Sensitivity analysis of the Biosphere-Atmosphere Transfer Scheme. *J. Geophys. Res.*, **101**, 7279–7289.
- Hack, J. J., 1994: Parameterization of moist convection in the NCAR Community Climate Model (CCM2). *J. Geophys. Res.*, **99**, 5551–5569.
- , B. A. Boville, B. P. Briegleb, J. T. Kiehl, P. J. Rasch, and D. L. Williamson, 1993: Description of the NCAR Community Climate Model (CCM2). NCAR Tech. Note NCAR/TN-382+STR, 108 pp. [Available from National Center for Atmospheric Research, Boulder, CO 80307.]
- Hahmann, A. N., D. M. Ward, and R. E. Dickinson, 1995: Surface land temperature and radiative response of the NCAR CCM2/BATS land scheme to modifications in the optical properties of clouds. *J. Geophys. Res.*, **100**, 23 239–23 252.
- Henderson-Sellers, A., 1992: Assessing the sensitivity of a land-surface scheme to parameters used in tropical deforestation experiments. *Quart. J. Roy. Meteor. Soc.*, **118**, 1101–1116.
- , R. E. Dickinson, T. B. Durbidge, P. J. Kennedy, K. McGuffie, and A. J. Pitman, 1993: Tropical deforestation: Modeling local to regional-scale climate change. *J. Geophys. Res.*, **98**, 7289–7315.
- Holtlag, A. A. M., and B. A. Boville, 1993: Local versus nonlocal boundary-layer diffusion in a global climate model. *J. Climate*, **6**, 1825–1842.
- Horel, J. D., A. N. Hahmann, and J. E. Geisler, 1989: An investigation of the annual cycle of convective activity over the tropical Americas. *J. Climate*, **2**, 1388–1403.
- Kiehl, J. T., 1994: Sensitivity of a GCM climate simulation to differences in continental versus maritime cloud drop size. *J. Geophys. Res.*, **99**, 23 107–23 115.
- , and B. P. Briegleb, 1991: A new parameterization of the absorptance due to the 15- $\mu$ m band system of carbon dioxide. *J. Geophys. Res.*, **96**, 9013–9019.
- Koster, R. D., and M. J. Suarez, 1995: Relative contributions of land and ocean processes to precipitation variability. *J. Geophys. Res.*, **100**, 13 775–13 790.
- Lean, J., and D. A. Warrilow, 1989: Simulation of the regional climatic impact of Amazon deforestation. *Nature*, **342**, 411–413.
- , and P. R. Rowntree, 1993: A GCM simulation of the impact of Amazonian deforestation on climate using an improved canopy representation. *Quart. J. Roy. Meteor. Soc.*, **119**, 509–530.
- , C. B. Buntun, C. A. Nobre, and P. R. Rowntree, 1996: The simulated impact of Amazonian deforestation on climate using measured ABRACOS vegetation characteristics. *Amazon Deforestation and Climate*, J. H. C. Gash, C. A. Nobre, J. M. Roberts, and R. L. Victoria, Eds., John Wiley, 549–576.
- Leemans, R., and W. P. Cramer, 1991: The IIASA database for mean monthly values of temperature, precipitation and cloudiness on a global terrestrial grid. International Institute of Applied Systems Analysis Research Rep. RR-91-18, Laxemburg, Austria, 61

- pp. [Available from IIASA, Schlossplatzl, A-2361 Laxenburg, Austria.]
- Legates, D. R., and C. J. Willmott, 1990a: Mean seasonal and spatial variability in global surface air temperatures. *Theor. Appl. Climatol.*, **41**, 11–21.
- , and —, 1990b: Mean seasonal and spacial variability in gage-corrected, global precipitation. *Int. J. Climatol.*, **10**, 111–127.
- Lenters, J. D., and K. H. Cook, 1995: Simulation and diagnosis of the regional summertime precipitation climatology of South America. *J. Climate*, **8**, 2988–3005.
- Manzi, A. O., and S. Planton, 1996: A simulation of Amazonian deforestation using a GCM calibrated with ABRACOS and ARME data. *Amazon Deforestation and Climate*, J. H. C. Gash, C. A. Nobre, J. M. Roberts, and R. L. Victoria, Eds., John Wiley, 505–529.
- McGuffie, K., A. Henderson-Sellers, H. Zhang, T. B. Durbidge, and A. J. Pitman, 1995: Global climate sensitivity to tropical deforestation. *Global Planet. Change*, **10**, 97–128.
- Mylne, M. F., and P. R. Rowntree, 1991: Modeling the effects of albedo change associated with tropical deforestation. *Climate Change*, **21**, 317–343.
- Nobre, C. A., P. J. Sellers, and J. Shukla, 1991: Amazonian deforestation and regional climate change. *J. Climate*, **4**, 957–988.
- Pitman, A. J., T. B. Durbidge, A. Henderson-Sellers, and K. McGuffie, 1993: Assessing climate model sensitivity to prescribed deforested landscapes. *Int. J. Climatol.*, **13**, 879–898.
- Polcher, J., and K. Laval, 1994a: The impact of African and Amazonian deforestation on tropical climate. *J. Hydrol.*, **155**, 389–405.
- , and —, 1994b: A statistical study of regional impact of deforestation on climate in the LMD GCM. *Climate Dyn.*, **10**, 205–219.
- Salati, E., 1987: The forest and the hydrological cycle. *Geophysiology of Amazonia. Vegetation and Climate Interactions*, R. E. Dickinson, Ed., John Wiley and Sons, 273–296.
- Sellers, P. J., 1992: Biophysical models of land surface processes. *Climate System Modeling*, K. E. Trenberth, Ed., Cambridge University Press, 451–490.
- Shaikh, M. J., 1996: Precipitation simulation in global climate models: Impact of horizontal resolution and improved land surface scheme. Ph.D. thesis, The University of Arizona, 246 pp. [Available from Dept. of Hydrology and Water Resources, University of Arizona, Tuscon, AZ 85721.]
- Shea, D. J., K. E. Trenberth, and R. W. Reynolds, 1992: A global monthly sea surface temperature climatology. *J. Climate*, **5**, 987–1001.
- Shuttleworth, W. J., J. H. C. Gash, J. M. Roberts, C. A. Nobre, L. C. B. Molion, and M. N. G. Ribeiro, 1991: Post-deforestation Amazonian climate: Anglo-Brazilian research to improve prediction. *J. Hydrol.*, **129**, 71–85.
- Sud, Y. C., G. K. Walker, J.-H. Kim, G. Liston, P. J. Sellers, and W. K.-M. Lau, 1996: Biogeophysical consequences of a tropical deforestation scenario: AGCM simulation study. *J. Climate*, **9**, 3225–3247.
- Trenberth, K. E., 1992: Global analyses from ECMWF NCAR Tech. Note NCAR/TN-373+STR, 191 pp. [Available from National Center for Atmospheric Research, Boulder, CO 80307.]
- Wright, I. R., and Coauthors, 1996: Towards a GCM surface parameterization for Amazonia. *Amazon Deforestation and Climate*, J. H. C. Gash, C. A. Nobre, J. M. Roberts, and R. L. Victoria, Eds., John Wiley, 473–504.
- Zeng, N., R. E. Dickinson, and X. Zeng, 1996: Climatic impact of Amazon deforestation—A mechanistic model study. *J. Climate*, **9**, 859–883.
- Zhang, H., K. McGuffie, and A. Henderson-Sellers, 1996: Impacts of tropical deforestation. Part II: The role of large-scale dynamics. *J. Climate*, **9**, 2498–2521.